REPORT DOCUMENTATION PAGE

Form Approved
OMB No. 0704-0188

1. AGENCY USE ONLY *(Leave blank)*	2. REPORT DATE	3. REPORT TYPE AND DATES COVERED
	5/14/2002	Final; 2/7/00 - 9/30/00

4. TITLE AND SUBTITLE
Sono Bus for Optical Data Distribution

5. FUNDING NUMBERS
DAAH01-97-D-R005
D.O. 024

6. AUTHORS
Scott Jeff Kulick

7. PERFORMING ORGANIZATION NAME(S) AND ADDRESS(ES)
UAH
Huntsville, AL 35899

8. PERFORMING ORGANIZATION REPORT NUMBER
N/A

9. SPONSORING/MONITORING AGENCY NAME(S) AND ADDRESS(ES)
US Army Aviation & Missile Command
Redstone Arsenal, AL 35898

10. SPONSORING/MONITORING AGENCY REPORT NUMBER

11. SUPPLEMENTARY NOTES

12a. DISTRIBUTION/AVAILABILITY STATEMENT
A

12b. DISTRIBUTION CODE

13. ABSTRACT *(Maximum 200 words)*

This report describes the results of a project to fabricate an integrated electro-optical assembly consisting of a photo detector array, fiber-optic v-groove package, and a fiber ribbon containing integrated Bragg grating output couplers. Assembly of each of the subassemblies was completed. Final assembly and testing of the integrated device is pended subject to the availability of better out-coupling behavior.

14. SUBJECT TERMS
Optical Interconnects
Manual Processing

15. NUMBER OF PAGES

16. PRICE CODE

17. SECURITY CLASSIFICATION OF REPORT	18. SECURITY CLASSIFICATION OF THIS PAGE	19. SECURITY CLASSIFICATION OF ABSTRACT	20. LIMITATION OF ABSTRACT
Unclassified	Unclassified	Unclassified	UL

DEFENSE TECHNICAL INFORMATION CENTER
REQUEST FOR SCIENTIFIC AND TECHNICAL REPORTS

Title Some Bits for Optical Data Distribution

1. Report Availability *(Please check one box)*

☑ This report is available. *Complete sections 2a - 2f.*

☐ This report is not available. *Complete section 3.*

2a. Number of Copies Forwarded 1

2b. Forwarding Date 5/14/2002

2c. Distribution Statement *(Please check ONE box)*

DoD Directive 5230.24, "Distribution Statements on Technical Documents," 18 Mar 87, contains seven distribution statements, as described briefly below. Technical documents MUST be assigned a distribution statement.

☑ DISTRIBUTION STATEMENT A: Approved for public release. Distribution is unlimited.

☐ DISTRIBUTION STATEMENT B: Distribution authorized to U.S. Government Agencies only.

☐ DISTRIBUTION STATEMENT C: Distribution authorized to U.S. Government Agencies and their contractors.

☐ DISTRIBUTION STATEMENT D: Distribution authorized to U.S. Department of Defense (DoD) and U.S DoD contractors only.

☐ DISTRIBUTION STATEMENT E: Distribution authorized to U.S. Department of Defense (DoD) components only.

☐ DISTRIBUTION STATEMENT F: Further dissemination only as directed by the controlling DoD office indicated below or by higher authority.

☐ DISTRIBUTION STATEMENT X: Distribution authorized to U.S. Government agencies and private individuals or enterprises eligible to obtain export-controlled technical data in accordance with DoD Directive 5230.25, Withholding of Unclassified Technical Data from Public Disclosure, 6 Nov 84.

2d. Reason For the Above Distribution Statement *(in accordance with DoD Directive 5230.24)*

2e. Controlling Office

2f. Date of Distribution Statement Determination

3. This report is NOT forwarded for the following reasons. *(Please check appropriate box)*

☐ It was previously forwarded to DTIC on ..... *(date)* and the AD number is .....

☐ It will be published at a later date. Enter approximate date if known. .....

☐ In accordance with the provisions of DoD Directive 3200.12, the requested document is not supplied because:

.....

.....

.....

Print or Type Name Jeff Kuiper

Signature JKP

Telephone 256 824 6019

(For DTIC Use Only)
AQ Number

Final Report

Jeffrey Kulick
Department of Electrical and Computer Engineering
The University of Alabama in Huntsville
Huntsville, Al. 35899

F/DOD/ARMY/AMCOM/SOME-Bus for Optical Data Distribution

Abstract

Work on this contract involved three subcontracts: fabrication of a detector array by Sensors Unlimited, fabrication of a mechanical package for integrating the detector array with fiber optics by Auburn University, and fabrication of slanted fiber Bragg gratings in the fiber optics by Alabama A&M University. Funding from this contract was primarily directed towards the fabrication of the detector array with additional funding being provided by a NSF EPSCOR grant.

Fabrication of these three sub-assemblies was completed. Figure 1 shows the physical layout of the detector array fabricated by Sensors Unlimited while Figure 2 shows the typical response for a single detector at data rates varying from 30 to 110Mhz.

Final reports from Auburn University and Alabama A&M University on the fabrication of the additional assemblies are attached as appendices.

Fabrication of these three assemblies took all of the allotted time and funding resources available and integration of these assemblies is pending further support.

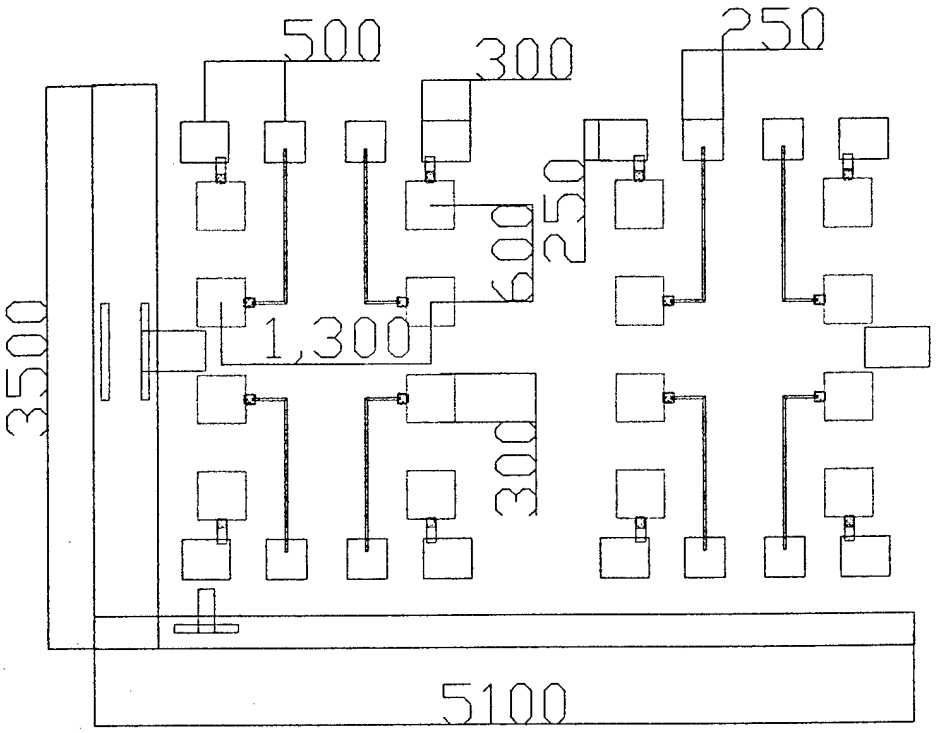

Figure 1 – Physical Layout of Sensors Unlimited Detector Array

Figure 2. Sensors Unlimited Detector Response

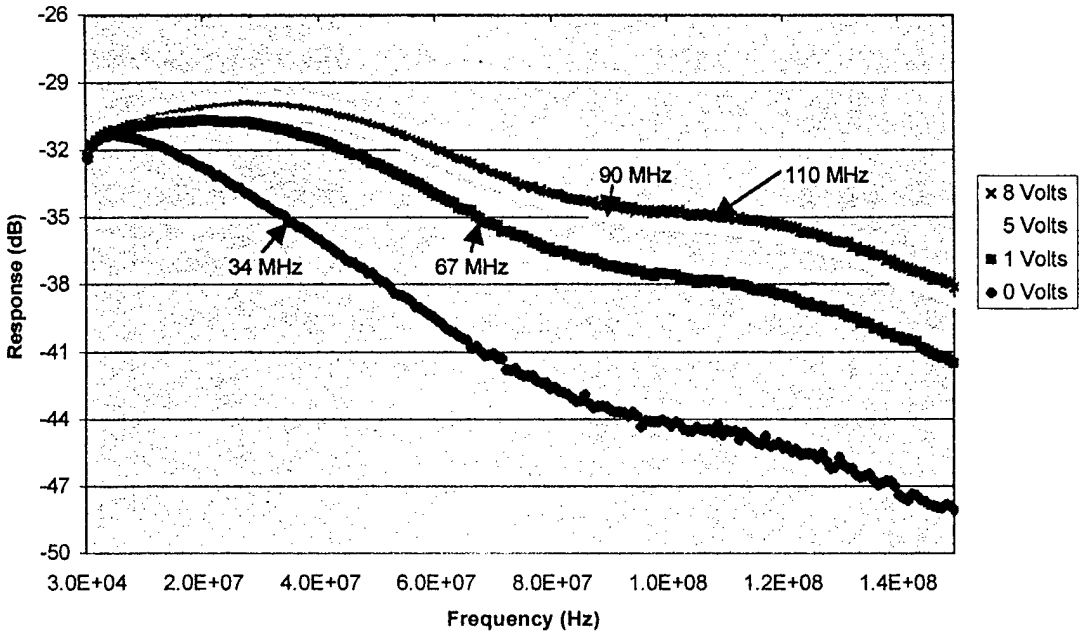

NFS EPSCOR - Optical Package for Integrated Detector CMOS Devices

Final Report

UAH-SUB2000-406-B

Ending - 6/30/2001

Principle Investigator: Charles Ellis
Auburn University
467 Broun Hall
Auburn, AL 36830
334-844-1883

INTRODUCTION

Microelectromechanical systems (MEMS) are microscopic devices with mechanical features constructed using techniques developed for integrated circuit manufacturing. Often, these devices are actuators which convert electrical signals into mechanical movement or sensors which convert mechanical forces into electrical signals. They may also be passive structures such as mirrors or V-grooves. Micromachining refers to the formation of mechanical features on a substrate by processes, such as etching, that alter the topography of the material.

The focus of this thesis is the design and construction of a MEMS device, using micromachining, to enable multiple optical fibers to be attached to a photo-receiver array without terminating the optical fibers. The scope includes the incorporation of the optical fibers into the MEMS device and the preparation of the assembly for holographic processing of the fibers, as well as preparation for attachment to the photo-receiver array. This device will be referred to as the fiber attachment device (FAD).

The impetus for developing the FAD is the proof of concept of a wavelength division multiplexed (WDM) optical fiber bus for a parallel processor computer system. This concept, known as The Simultaneous Optical Multiprocessor Exchange Bus (SOME-Bus), was developed by University of Alabama Huntsville Faculty [1]. The concept requires that the signals in each fiber be de-multiplexed at each processor. To accomplish this in a reasonable amount of space, the de-multiplexer cannot consist of discrete components. So, the de-multiplexing is to be accomplished by inscribing gratings in the fibers themselves to divert samples of light of each particular wavelength to a corresponding photodetector. The photodetector and FAD assembly is to attach directly to the processor die as shown in Figure 1. As the purpose of the FAD is to facilitate the alignment of the fibers for inscription of the gratings and facilitate the alignment and attachment of the fibers to the detector array, its development is an integral step in the proof of the SOME-Bus concept.

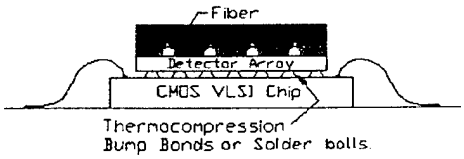

Figure 1. Fiber Attachment Device

The developmental stages for the FAD were: definition of device requirements, choice of manufacturing technique, mask design, mask layer growth, photolithography, etching of mask layer, etching of substrate, preparation of fiber, attachment of fiber, grinding, and polishing, and testing. The mask design was also used in the development of the detector array.

The SOME Bus developers defined the requirements of the FAD as follows:

1. Detector array must attach to a proof-of-concept processor die 4.5 x 4.5 mm.
2. Allow for wire bonding along two sides of processor die.
3. Attach four optical fibers to the detector array.
4. Provide for alignment to detector array.

The precision required for the alignment of the fibers makes silicon micromachining an ideal technique for the development of the FAD. Knowledge of the crystalline nature of silicon allows for predictable anisotropic etching of a substrate in liquid etchants (wet etching). Wet etching of a patterned substrate does not require expensive equipment. For this reason, the FAD was designed to use anisotropic wet etching to form parallel V-shaped grooves to form precisely spaced beds for the optical fibers. Because the geometry of the grooves is predictable, the depth of the fiber below the surface of the substrate can also be precisely controlled.

Several parts can be simultaneously fabricated on a single silicon wafer. After the parts are separated by sawing, the fibers can be laid into the grooves with an adhesive material to secure them. Because the fibers are round, the part of the fibers that lies above the surface of the silicon must be ground flat and polished to provide for mating to the detector array. Controlling the dimensions of the V-grooves controls the distance from the light-carrying core of the fiber to the flat surface. This core to surface dimension is important in the optical calculations required for writing the gratings and for designing the detector array.

METHOD OF WORK

1.1 Design of Device

The most suitable substrate material for the construction of the FAD V-groove device is <100> silicon. <100> silicon allows for the etching of V-grooves with a potassium hydroxide (KOH) wet solution. To allow for the possibility of through-wafer alignment methods to align the FAD to the detector array, it is also desirable to have the wafers polished on both sides. Most laboratory tooling for MEMS devices, including the equipment at Auburn University, allows for the use of 100 mm (4 inch) wafers. For these reasons, 100 mm <100> silicon wafers were chosen for the fabrication of the FAD.

A criterion of the design was to remove the cladding material from the optical fiber to within 9 to 15 microns from the core of the fiber. The optical fiber to be used, Corning SMF-28, has a 9 micron diameter core, a 125 micron diameter cladding, and a 250 micron diameter plastic coating. The plastic coating can be removed with mechanical or chemical stripping, but the cladding which is composed of silica must be removed by grinding and polishing techniques. This was accomplished by sizing the grooves so that the fibers would rest in the grooves while the exposed part of the fiber

could be removed with mechanical grinding and polishing. Figure 2 illustrates how a stripped fiber would lay in a V-groove. The groove sidewall slope is determined by the crystal properties of the substrate and is 54.74 degrees. To obtain the V-shaped groove, the groove must be etched until the <111> crystal planes meet. Etching will cease at this point due to the selectivity of the etchant. Therefore, the etch depth and, ultimately, fiber depth is controlled by the width of the V-groove.

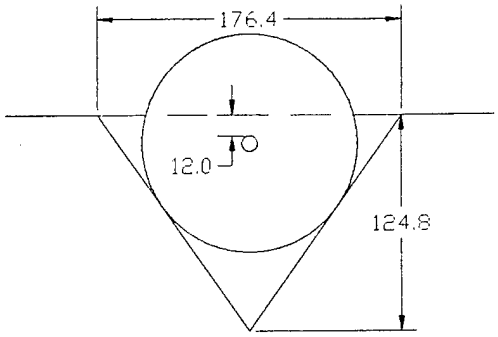

Figure 2 V-groove depth

Some simple trigonometry is involved in calculating the groove width. First the desired depth below the substrate surface of the center of the fiber must be determined. This is given by

$$fd = t_{cladding} + r_{core} \qquad \textbf{(1.1)}$$

where $t_{cladding}$ is the desired thickness of the cladding, and r_{core} is the radius of the core. Following Figure 3, the height of the center of the fiber above the groove bottom is given by

$$h = \frac{r}{\cos(54.74^{o})} \qquad \textbf{(1.2)}$$

where r is the radius of the cladding. The depth of the grove and width of the groove are given by

$$d = h + fd \qquad \textbf{(1.3)}$$

and

$$w = 2\frac{d}{\tan(54.74^{o})} \qquad \textbf{(1.4)}$$

respectively.

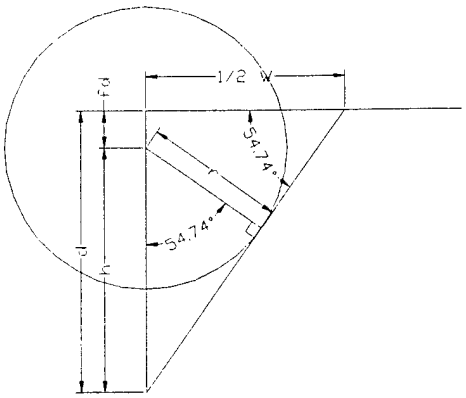

Figure 3 Groove Geometry.

The VLSI test chip was designed to comply with the MOSIS fabrication specifications. Because of this, the die size was limited to 4.5 x 4.5 mm. As shown in Figure4, the detector array and FAD were designed to attach to the top of the test die. The electrical connections from the test detector array to the test die were to be made using flip chip technology via solder bump bonds or thermocompression bonding. The FAD and detector array were designed to allow for wire bond connections to be made from the test die to the hybrid circuit board or chip carrier.

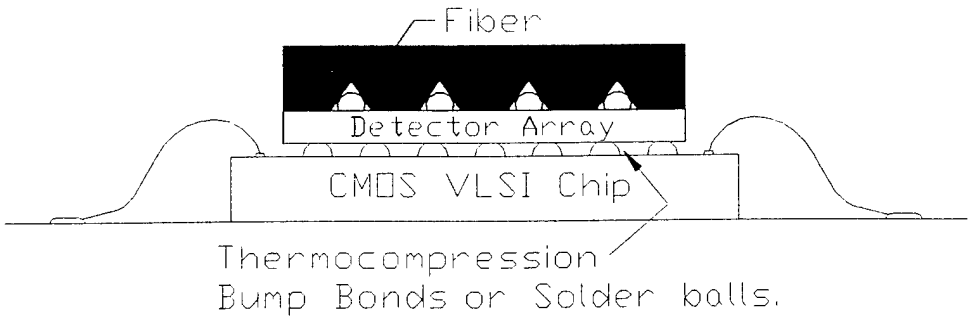

Figure 4. Conceptual Side View

To allow the fibers to extend from each end of the fiber attachment device as necessary to form a bus, the wire bond pads are along only two sides of the VLSI test chip. This also limits the size constraint of the FAD and detector array to only one dimension. The FAD can be extended along the fiber axis to provide for strain relief of the fibers as illustrated in Figure5. The FAD is shown in red.

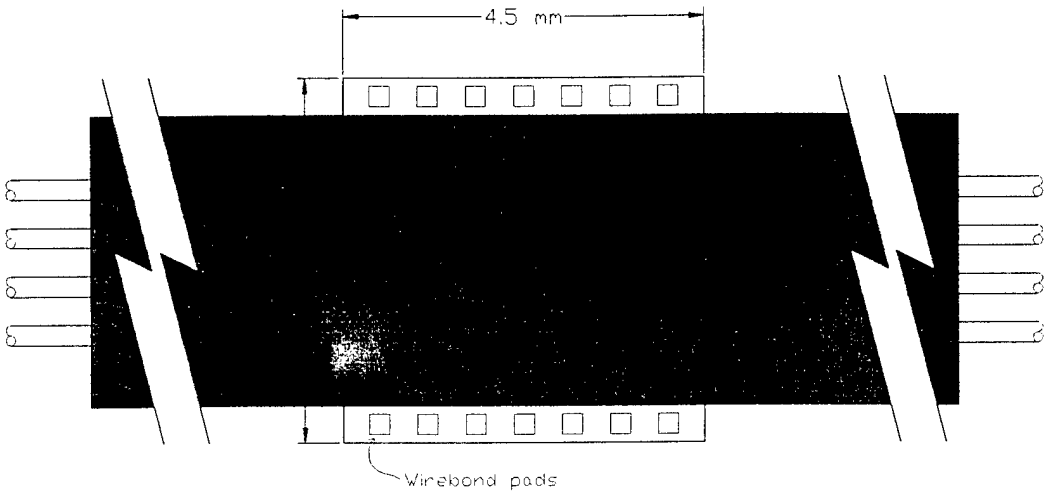

Figure 5. Conceptual Top View

The portion of the fiber to be in contact with the detector array is stripped of the plastic coating. The stripped fiber is very brittle. To provide for strain relief, the FAD employs an extension of the grooves beyond the area which will contact the detector array. The extended grooves were designed to accommodate the un-stripped fiber while maintaining the axis of the fiber. The calculations for the width of the groove extensions are identical to those above except that the radius of the fiber with coating is 125 microns.

With the above constraints in mind, the FAD was designed to be 3.6 mm wide and 63.5 mm long. The pitch of the four optical fibers was specified to be 0.6 mm. The target width for the V-groove containing the sheathed optical fiber was 329.5 microns and the target width of the V-groove receiving the stripped portion of the optical fiber was 176.4 microns. As in integrated circuits, several MEMS devices can be simultaneously fabricated on each silicon wafer. In the case of the FAD, there was room on the 100 mm diameter wafer to place nine devices.

1.2 Process Definition

In order to use wet etching to form the V-grooves, it is necessary to mask the areas of the substrate that will not be etched while providing the etchant access to the portions of the substrate to be etched. For many wet etching processes, the masking material is photoresist, a family of polymer coatings that can be applied to a wafer and patterned photographically so that areas of the coating are removed during a developing

process. When KOH etching is used, however, photoresist is inadequate as an etch mask. Photoresists are typically incompatible with alkaline etchants, and deep V-grooves require an etch 6-8 hours in duration. A suitable mask for KOH etching is Silicon Nitride (Si3N4) which is formed on the wafers using a low pressure chemical vapor deposition process (LPCVD). This mask is patterned with normal photolithography techniques and reactive ion etching. Si3N4 deposition is usually proceeded by a chemical vapor deposition of silicon dioxide.

It is necessary to dice the wafers prior to placing the fibers in the v-grooves. The grinding and polishing must, of course, occur subsequent to placing the fibers in the v-grooves. The exposed fiber pigtails are susceptible to stress fractures where the fibers enter and exit the FAD. A table of the process steps is listed below.

Step	Step Name	Mask Required
1	Thermal Oxidation	
2	LPCVD Nitride	
3	HMDS Vapor Prime	
4	Spin on Photoresist	
5	Expose	V-groove etch wells
6	Develop Photoresist	
7	Oxygen Plasma Descum	
8	Nitride Etch	
9	Buffered Oxide Etch	
10	Photoresist Strip (Acetone/Methanol)	
11	Piranha Clean (Sulfuric/Hydrogen Peroxide)	
12	KOH Etch	
13	DI Rinse	
14	Cut Fiber Sections	
15	Strip Center of Fiber Sections (4.5 mm)	
16	Dispense Epoxy Into V-groove	
17	Place Fiber in Groove	
18	Cure Epoxy	

19	Grind	
20	Polish	

With these steps defined, mask layout and process development can occur.

1.3 Mask Layout

As mentioned previously, multiple parts (dice) can be fabricated simultaneously on each wafer. When developing a new process, it is often desirable to design the mask such that certain parameters are varied from die to die, or from one region of the wafer to another. The process flow of the FAD reveals three etching steps. If any of these steps produce undercutting of the mask material due to anisotropy or reduced selectivity, the V-groove dimensions could be affected. In addition, it was possible for the epoxy in the grooves to prevent the fiber from seating as far into the grooves. It was chosen, therefore to vary the etch window openings in the mask layout bracketing the target V-groove dimensions in 5 micron steps. There was enough room for nine dice on each wafer. The target size, and four on either side. An Excel spreadsheet was composed to organize the dimension data for the different die see Table 1. The spreadsheet was designed to aid in layout by giving the "x" coordinates of the feature corners on each die as illustrated in rough sketch in Figure6. Dimension "a" is the wide groove dimension, and "b" is the narrow groove dimension.

Table 1. Mask Groove Dimensions

Dimensions										
a	b	c	d	e	f	g	h	i	j	die number
309.5	156.4	276.65	353.2	519.6	431.4	586.15	509.6	210.1	363.2	0
314.5	161.4	274.15	350.7	519.6	431.4	588.65	512.1	205.1	358.2	1
319.5	166.4	271.65	348.2	519.6	431.4	591.15	514.6	200.1	353.2	2
324.5	171.4	269.15	345.7	519.6	431.4	593.65	517.1	195.1	348.2	3
329.5	176.4	266.65	343.2	519.6	431.4	596.15	519.6	190.1	343.2	4
334.5	181.4	264.15	340.7	519.6	431.4	598.65	522.1	185.1	338.2	5
339.5	186.4	261.65	338.2	519.6	431.4	601.15	524.6	180.1	333.2	6
344.5	191.4	259.15	335.7	519.6	431.4	603.65	527.1	175.1	328.2	7
349.5	196.4	256.65	333.2	519.6	431.4	606.15	529.6	170.1	323.2	8

LASI 6.0 software was used for the mask layout. This software is free to not for profit organizations and is available on the internet. The base drawing units were chosen to be microns. Each die was designed as a cell. The cells were then placed within a higher rank cell to form the array of die which is the mask layout. The die with the most narrow and shallow grooves is on the left, and the die with the widest grooves is on the right.

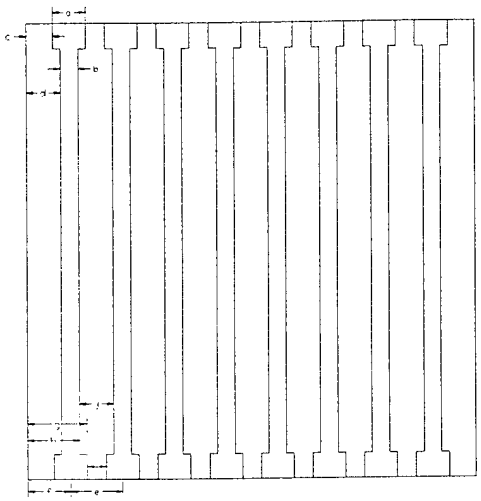

Figure 6. Layout Sketch

As discussed previously, the wide grooves extend well above and below the area which contacts the array. Each narrow groove was designed to be 3600 microns in length while the wide grooves extend 29950 microns (~3 cm) in each direction.

In addition to defining the etch window the mask layout also provides alignment marks for mating the FAD to the detector array and a set of marks that form a binary code to identify each die. The identification marks are necessary so a die's groove size can be easily identified after the wafer is sawn. The I.D. pattern is formed by a vertical array of four objects. If an object is a rectangle, it represents a zero. A square represents a one. The bottom object is the least significant digit. This is aptly illustrated in the upper left-hand corner of Figure7. which is die number three and is identified by a binary 11.

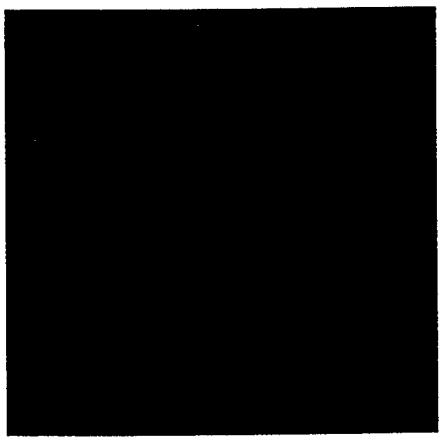

Figure 7. Die 3 Layout

The LASI file was converted to GDSII file format and sent to Harris corporation in Melbourne, Florida for mask fabrication. The four inch mask for contact mask alignment is a chrome on quartz mask. The data (shown in green) defines the transparent area of the mask because it was designed for use with positive photoresist. Areas of positive photoresist that have been exposed to light in a mask aligner are dissolved by developer.

1.4 Oxide and Nitride Deposition

As mentioned before, Silicon Nitride, Si3N4 is used as a mask layer for KOH etching. Silicon Nitride is deposited on Silicon using low pressure chemical vapor deposition (LPCVD). However, it is common practice to grow a layer of Silicon Dioxide prior to SiN_3 for the purpose of strain relief.

The Silicon Dioxide was grown using a wet thermal oxidation process in Auburn's Tylan CVD furnace. Wet oxidation uses hydrogen gas to speed up the oxide formation. The furnace consists of a quartz tube heated by jacket heating elements. Gases are passed through the tube via mass flow controllers. The tube interior is always at atmospheric pressure, but a Nitrogen ambient is maintained when deposition is not occurring. The parameters were set as follows:

Parameter	Value
Temperature	1000° C
O_2 Hi	2.97
O_2 Lo	1.46
H_2	0.6
Time	20 min
Load Speed	3

The wet oxidation time of 20 minutes is preceded and followed by 5 minute periods of time when oxygen is applied without the hydrogen (dry).

Silicon Nitride is deposited on the wafer using dichlorosilane in a LPCVD furnace.

1.5 Photolithography

Photolithography is the process of patterning photoresist on a wafer. Prior to the application of photoresist, the surface of the wafer is treated in a vapor priming process. This is accomplished by placing wafers in a chamber that is heated to 150° C and cycled through 3 vacuum and nitrogen purge cycles to dehydrate the Silicon. The vacuum is on the order of 1 mTorr. Then, HMDS vapor is applied to the wafer at reduced pressure (~6 Torr).

1.5.1 Spin and Soft Bake

The photoresist is applied by pooling it on to the center of the wafer and spinning the wafer at high speeds (3000 rpm in this case). The spin speed and photoresist viscosity determine the thickness of the coating. The spin time was 30 seconds. The resist used for the FAD nitride patterning was AZ5214. After spinning on the resist, it is critical to avoid exposing the wafers to any light (other than yellow light) until the photoresist is developed. To solidify the coating by vaporizing the volatile solvents, the wafers were soft baked in a 90° C convection oven for 30 minutes.

1.5.2 Exposure

The exposure was accomplished with a Karl Suss contact mask aligner. With a contact mask aligner, the chrome side of the mask makes solid contact with the photoresist surface. The pattern feature size is virtually the same as the mask feature size. The ultra-violet light source is a mercury vapor lamp. Usually, for a first pattern, alignment is not necessary other than properly placing the wafer on the chuck of the mask aligner to make subsequent alignments easier. In the case of the FAD, however, it was necessary to ensure that the theta (rotation) axis of each wafer was such that the wafer flat was aligned to the top edge of the mask holder. This step is necessary because the V-grooves etch windows must be aligned with the edge of a (111) crystal plane. The exposure time was 30 seconds.

1.5.3 Develop and Hard Bake

The photoresist was developed in a 4:1 water to developer solution for 1 minute. The developed pattern was visually inspected before hard bake. The wafers were hard baked in a 120° C oven for 30 minutes to cross-link and harden the photoresist.

1.6 Nitride and Oxide Etches

The V-groove etch window pattern is transferred from the photoresist into the Si3N4 layer by etching the exposed Si3N4 in a Matrix 303 etcher. The Matrix uses a plasma of CF_4 to etch the Silicon Nitride. Because the plasma can affect the backside of the wafer, it was protected by taping the backside of each wafer with tape that is manufactured for mounting wafers for dicing. The etching parameters were as follows:

Parameter	Value
O_2	10 %
CF_4	40 %
Pressure	1.30 Torr
Power	300 Watts
Chuck Temperature	100° C

It was then necessary to remove the exposed SiO_2 layer that was underlying the SiN_3 because SiO_2 etches much slower than Silicon in KOH. After removing the tape

from the back side of the wafer, the SiO_2 was etched in a one minute dip in a buffered oxide etch (BOE). The BOE is a buffered hydrofluoric acid (HF) solution.

It is desirable to strip the photoresist from the wafer before the KOH etch. The photoresist would not be of any benefit in the KOH bath and would only serve to contaminate the etching solution. The photoresist was stripped with an acetone rinse followed immediately by a methanol rinse. A hot bath of 70% Sulfuric acid and 30% Hydrogen Peroxide was used to remove any organic residues from the wafer prior to the KOH etch.

1.7 KOH Etching

The 45% KOH solution was prepared in a 3000 ml beaker and consisted of 625 ml of de-ionized water (DI), 1000 ml Potassium Hydroxide (KOH), and 600 ml 2-propanol. The solution was placed on a hot plate and heated to 80° C and agitated with a stirrer bead. The top of the beaker was covered with a large watch glass.

The wafers to be etched were placed in a Teflon wafer boat and lowered into the solution. The etching progress was monitored by removing the wafers, rinsing and drying one, and examining the etch depth under a microscope. The etch depth was checked by focusing on the wafer surface, noting the micrometer reading on the fine focus knob, then focusing on the bottom of the groove or pit and noting the micrometer reading. The difference in the readings is the depth of the groove. Etch rates were monitored so that an accurate projection of end time could be made as the etch runs progressed. After etching, the wafers were rinsed in a cascading DI bath.

The wafers were mounted on tape and diced on Auburn University's diamond wafer saw. The saw was aligned to the alignment marks on the wafer.

1.8 Mounting the Optical fiber

The optical fiber was cut into 24" lengths so that the fiber would extend well beyond the length of the FAD to provide "pig tails" for attaching test instrumentation. A Miller Stripper was used to remove the plastic coating from the middle 5 mm each piece of fiber. The Miller Stripper is a mechanical stripper which has a 0.14 mm laser drilled hole. It is hand-held, looks, and is used very much like wire strippers. Unlike wire strippers, which must be used at the terminus of a wire, the Miller stripper can be used to remove a portion of coating anywhere along the length of a fiber.

Norland Optical Adhesive was dispensed using a 3 cc syringe with a blunt 1.2 mm needle. After dispensing adhesive into a V-groove, the fiber was placed into the groove. When all four grooves of a die were filled, the edge of a glass microscope slide was passed along the length of the die as a doctor blade to remove the excess epoxy. A clean slide wrapped in Glad plastic wrap was used to clamp the fibers securely into the grooves while the epoxy was cured with a Fiber Instrument Sales WO-1067 UV lamp for 5 minutes. The plastic wrap prevents the epoxy from adhering to the slide.

1.9 Grinding and Polishing

Grinding is a process that employs fixed abrasives to remove material from a surface. The vehicle for the abrasives is often paper or film. The principle variables affected by grinding are the height of the ground surface, and the flatness of the surface. In general, grinding can be used to make a surface flatter. In the case of the FAD, grinding was used to remove the cladding of the fiber which was exposed above the Silicon surface. This was necessary not only to remove the cladding, but to provide a flat surface for mating to the detector array.

The polishing process generally employs abrasives in the form of a slurry or paste in loose form to improve the finish of a surface. The slurry is often worked into a soft pad. The surface to be polished is then rubbed against the pad. Polishing is used to remove the surface damage caused by grinding. The principle variable affected by polishing is RMS, a measure of surface quality. The purpose of polishing the top surface of the FAD is to eliminate any diffraction of light that has been coupled out of the fiber.

Several methods were evaluated for grinding and polishing the optical fiber. The first was the FIS hand polishing system designed for use with fiber optic connectors. It utilizes two polishing films on a soft rubber backing. The coarse film has 5 micron abrasive particles, and the coarse film has 1 micron abrasive particles. There are many variables with this system such as polishing time, pressure, and film usage.

An automated system for preparing metallurgical cross section samples was available. The Buehler Ecomet 6 system with the Automet 2 power head shown in Figure 8. provided the potential for a repeatable grinding and polishing process where the parameters were machine controlled.

The system provides two spindles for abrasive discs or polishing pads. Speed control and cooling/cleaning water are provided for the spindles. The Automet head provides a spinning chuck for the mounting of a sample holder. The chuck spins at a constant speed of 60 rpm. Downward force is applied by the chuck and is controllable in 1 lbf increments starting at 1 lbf.

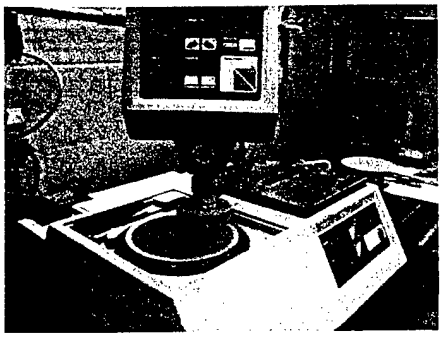

Figure 8. Buehler Ecomet 6

A great deal of process development was required for the grinding/polishing step. The unusual aspects of this process were that the wafer was diced prior to polishing and that the parts each had four optical fibers protruding from each end. In addition, the inhomogeneous combination of the silica fiber and the silicon FAD make the selection of abrasives difficult. The abrasive must be harder than the material being ground. However, the geometry of some abrasives can cause brittle material to fracture as it is ground. If silicon carbide is used to grind silica, care must be taken to avoid this problem.

The only fixture readily available for the chuck was a fixture for grinding and polishing 1.5 inch round cross section samples. So, it was necessary to develop a fixture for the FAD. Figure9. shows the results of using an early attempt at a fixture which was machined by the author in Auburn's Electrical Engineering machine shop. A portion of a broken FAD is visible near the center of the fixture. It is obvious that the FAD parts are brittle and require a flat support during polishing.

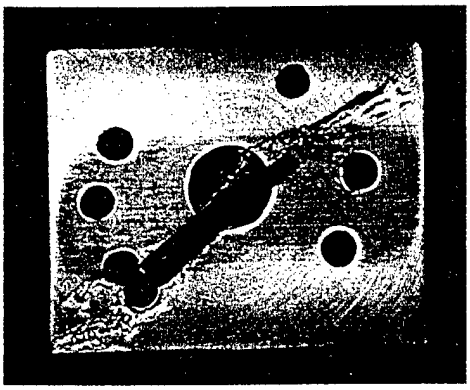

Figure 9. Early Grinding Fixture

A round fixture had been designed by Michael Palmer of Auburn's electronics packaging group for polishing 100 mm wafers. This fixture was evaluated for use with the FAD. It was found that the un-protected fiber pig tails were often broken during processing even when secured with tape to the side of the fixture as shown in Figure 10.

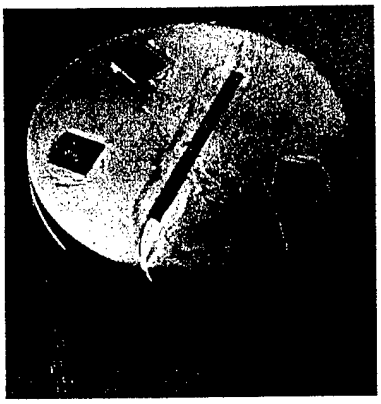

Figure 10. Round Grinding/Polishing Fixture

In an attempt to solve this problem, a tray was machined into the fixture for each set of pig tails. The tray served as a transition from the front of the polishing fixture to the side. Figure 11. shows a portion of the engineering drawing prepared for the machine shop. The fibers could actually be held in the trays with wax to protect them during grinding/polishing.

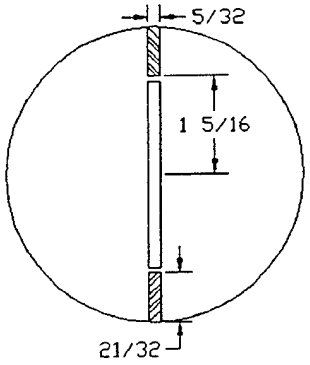

Figure 11. Modified Grinding Fixture

To achieve faster results, rough grinding can be performed at higher wheel speeds than those use for fine grinding. For 400 and 1200 grit silicon carbide (SiC) paper, 240 rpm was used. For 2400 grit (SiC), 120 rpm was used. The SiC pads were round pads from Buehler, the makers of the grinding machine. In addition to the SiC pads, some diamond pads from Buehler were evaluated. Polishing was accomplished with Buehler Texmet 1000 polishing pad and 0.1 micron paste.

RESULTS AND CONCLUSIONS

2.10 Introduction

The results are presented in a manner that allows them to be associated with the appropriate process steps. While some results were incorporated into process development, others will be useful in future process development.

2.11 Mask Layout and Lithography

The layout of the device provided nine different groove sizes. The target design width was 176.4 microns for the narrow portion of the grooves and 329.5 microns for the wide portion of the grooves. There are four grooves either side of center. They bracket the center dimension by 20 microns on either side in 5 micron increments. After etching, the dimensions of grooves of several die from several wafers were examined. The dimensions were measured on a Nikon microscope with encoders on the movable stage. The results were favorable in most respects.

On every wafer measured, the distance between grooves (pitch) was 600 microns as designed. The measured widths were greater than designed. The lengths of the wide part of the grooves were also somewhat greater than the mask layout. The widths of several the grooves for several wafers are plotted in Figure 112.

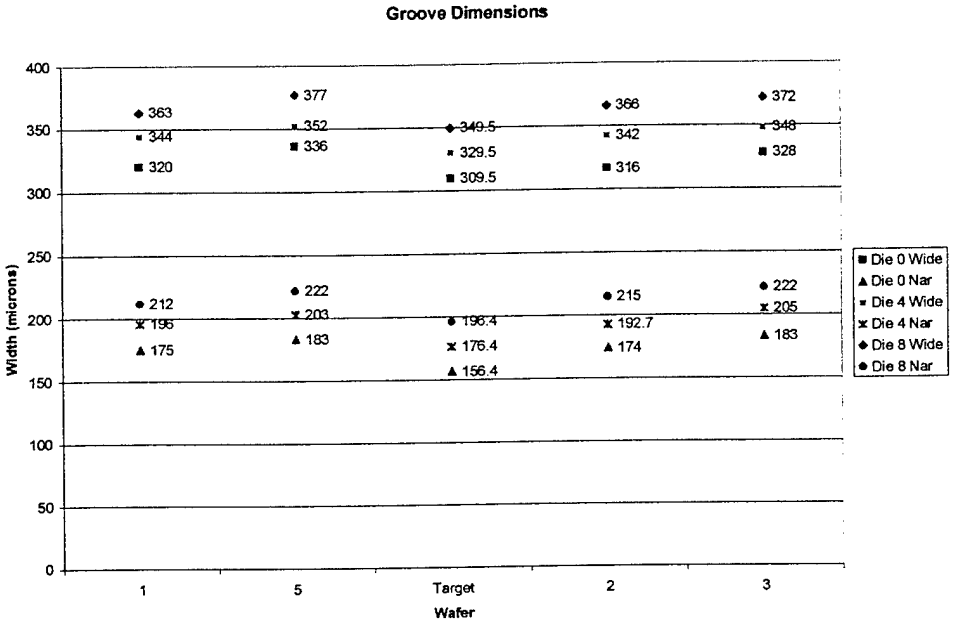

Figure 12. Groove Width Data

There are two probable causes for the groove width exaggeration. The photoresist layer was undercut during the silicon nitride etching or the mask was misaligned to the

(110) crystal direction. Any misalignment could cause undercutting of the nitride mask during KOH etching as illustrated in Figure 13. The blue square represents the silicon nitride mask window. The black outline represents a V-groove etched to completion. Etching propagates horizontally under the mask at the (100) etch rate until an un-broken (111) plane is encountered. The maximum increase in width is given by,

$$\frac{w}{w_0} = \cos(\theta) + \frac{L_0}{w_0}\sin(\theta) \qquad \textbf{(2.1)}$$

where w is the etched width, w_0 is the mask width, and θ is the angle of mask misalignment. In the case of grooves with such a high aspect ratio, a small misalignment can cause a significant width deviation.

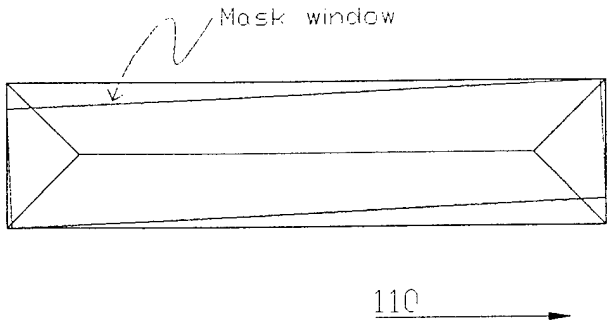

Figure 13. Mask Misalignment

The recommended solution for this problem is to design a mask with two circular windows near the edge. These circular etch windows would produce shallow pyramidal pits during a short KOH etch. The bottom edges of the pit could then be used to align the V-groove etch mask to the correct crystal orientation.

Data on groove depths were also taken after etching and are displayed in

Figure 14. The variation in groove depth is, of course, determined by the groove width. The solution recommended to control the groove width should also control the groove depth.

The fiber depth in the grooves can only be determined after the polishing step because it is not known how the fiber mounting process affects fiber core depth below the surface of the silicon. Possible effects are displacement of the fiber by a layer of epoxy on the walls of the grooves, expansion of the epoxy after curing, and variations in the clamping technique during epoxy curing.

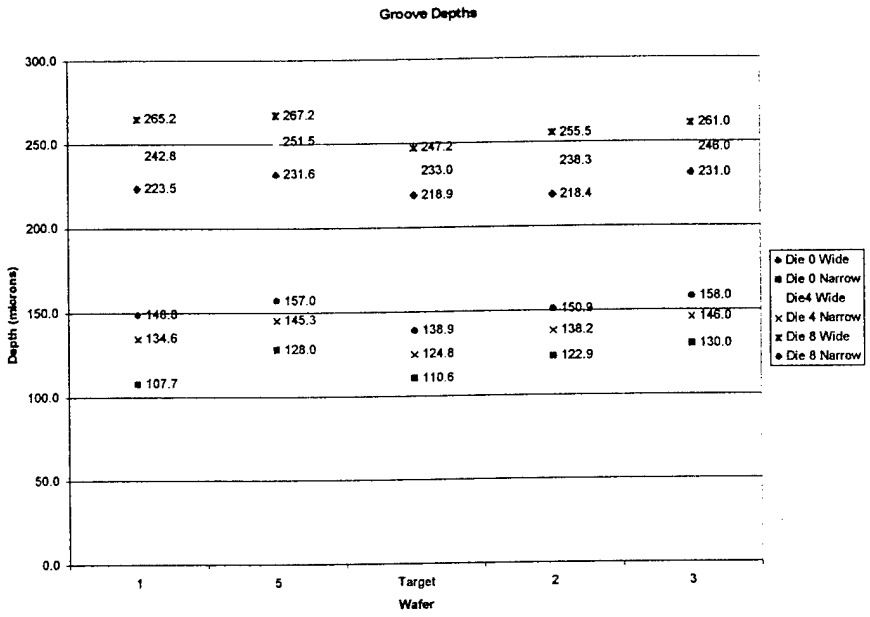

Figure 14. Groove Depth Data

To check the depth of the fiber core within the grooves of the FAD, two methods were used. The first was to measure the width of the ground and polished fiber surface. This was done on the Nikon microscope with the movable stage. The depth of the fiber could be estimated as

$$fd = \sqrt{r_{clad}^{\ 2} - \left(\frac{w}{2}\right)^2} \qquad \textbf{(2.2)}$$

$$d_{core} = fd - r_{core} \qquad \textbf{(2.3)}$$

where fd is the depth of the fiber center, r_{clad} is the radius of the cladding, and w is the width of the polished surface as illustrated in Figure 15. In (2.3), the depth of the core (d_{core}) is obtained by subtracting the core radius from the fiber center depth.

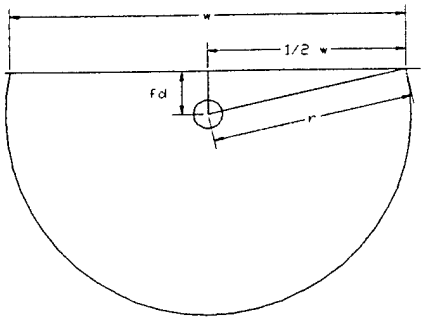

Figure 15. Depth from Width

This was verified by cross sectioning several samples. Cross sectioning is a destructive test method which involved scribing and breaking a polished FAD in the middle. The broken halves were then placed in cylindrical molds and held vertical with a sample clip. Then, a potting compound of 5:1 Buehler Epo-Kwik epoxy resin and hardener were poured around the sample and cured. The resulting form was then removed from the mold and ground to obtain un-damaged fiber and polished. It was necessary to polish both sides of each sample so that light could couple into the fiber core when the sample was viewed with transmitted light microscopy. Figure 16. is a micrograph of a cross-sectioned sample with a clearly visible fiber core. This section is of the narrow groove portion of the FAD, thus the plastic coating has been removed from this portion of the fiber. The UV curable epoxy is visible at the vertex of the V-groove.

The depth of the core was measured on the American Optical Epi-Star trinocular microscope. The vertical ocular provides a scale for measuring features in the field of view. The sample shown in Figure 16. is from wafer 3, die 4. The core depth (thickness of the ground cladding) measured was 19 microns. This falls outside the specified range of depths (9-15 microns).

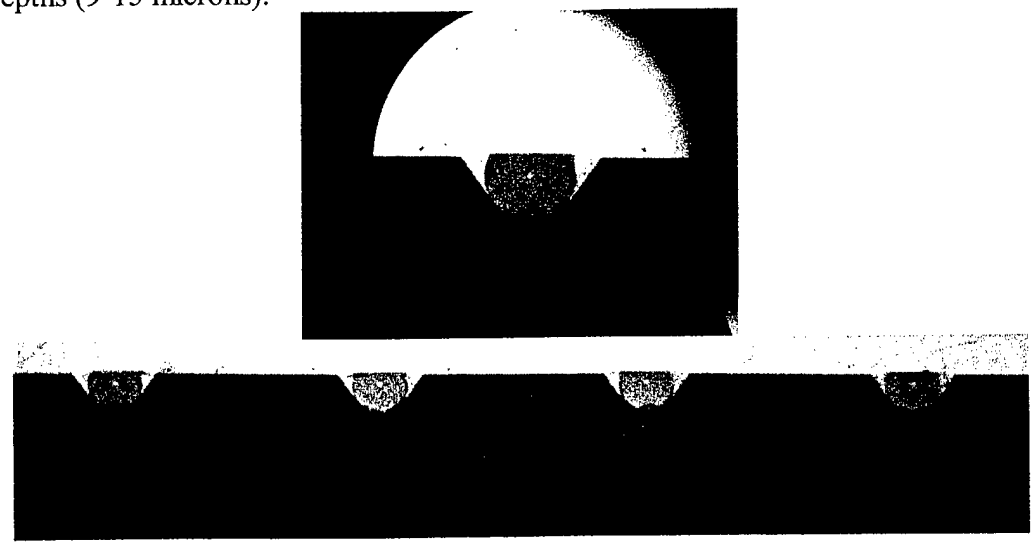

Figure 16. Cross-sectioned Sample

The distance from the vertex of a groove to the center of the fiber resting in a groove is given by (2.2). The depth of the fiber center is given by

$$fd = \frac{w}{2}\tan(\theta) - \frac{r}{\cos(\theta)} \qquad \textbf{(2.4)}$$

and the core depth is given by

$$d_{core} = \frac{w}{2}\tan(\theta) - \frac{r_{clad}}{\cos(\theta)} - \frac{r_{core}}{2} \qquad \textbf{(2.5)}$$

Because the fiber dimensions and the slope of the v-grooves are constant, the core depth varies with the groove width as

$$\frac{\partial d_{core}}{\partial w} = \frac{1}{\sqrt{2}} \qquad \textbf{(2.6)}$$

so the bracketing of groove widths (+/- 20 microns) should bracket the fiber depth well enough (+/- 14 microns in 3.5 micron steps) to provide useful die from die 1 to die 2.

2.12 Etching

2.12.1 Silicon Nitride Etching

The Silicon Nitride reactive ion etching was successful at first attempt. The process was already in use at Auburn. Surface roughening of the silicon was visible to the bare eye. Further process development would involve tuning the etching process (duration) to the thickness of the nitride layer. In addition, it may be possible to tune other process parameters to improve the selectivity for nitride over silicon.

2.12.2 KOH Etching

The etch rates observed during KOH etching were comparable to those predicted in the literature review. The etch rates varied from 35 microns/hour (0.6 microns/minute) to 41 microns/hour (0.7 microns/minute). The etch rate was monitored by removing the wafers from the etchant and checking their depth. This was accomplished by reading the micrometer on the fine focus knob on the A/O Epi-Star with the 40X objective while focusing on the surface and while focusing on the bottom of the groove. The difference between the two readings gave the etch depth. The total etch time for each run was 6 to 7 hours. Although the etch was self stopping, it was desirable to remove the wafers from the etchant as soon as the etch was complete.

The surface roughness was completely acceptable for the application of the FAD. No large hillocks were observed. Pitting was observed on areas of the wafer that should not have been etched. This is probably due to pin-holes in the nitride mask. A thicker or more uniform nitride layer should eliminate this problem.

Process improvements for KOH etching involved implementing a reflux cap to reduce the evaporation of the 2-propanol and the use of an Techne Tempette TP-8D oil bath to better control the etch temperature. The oil bath and reflux system can bee seen in Figure 17.

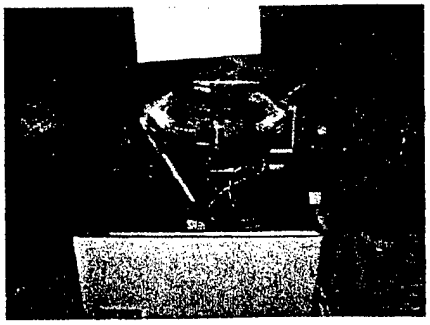

Figure 17. Oil Bath

2.13 Grinding and Polishing

Grinding and polishing have been the most challenging processes to develop. The primary challenge is protecting the die and fibers from breakage during the process. As mentioned before, the grinding and polishing steps must occur after the optical fiber has been epoxy attached to the grooves. It is also subsequent to wafer dicing because the dicing must occur before fiber attach. This is because the very ends (0.5 mm) of the die must be removed during dicing to obtain open-ended V-grooves.

2.13.1 Hand Lapping

The first attempts at grinding and polishing involved hand polishing using the Fiber Instrument Sales FI-9799 hand polishing system see Figure 18. The hand polishing system consists of a box containing a roll of lapping film which is scrolled across a rubber pad on top of the box and onto a take-up roll inside the box. The two-part film has 5 micron and 1 micron abrasive particles. This system was designed for polishing the connectorized ends of optical fiber while the connector is attached to a polishing disc.

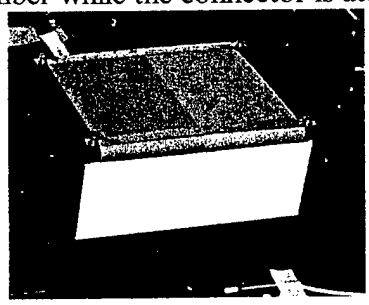

Figure 18. Hand Polishing System

This system was difficult to use for grinding and polishing of the FAD for two reasons. It was difficult to control the polishing parameters such as speed and pressure because they are determined by the user. In addition, it provided for very slow material removal. If the operator used close to the maximum pressure that could be applied without fracturing the FAD, it took about 30 minutes to polish a part to completion. Using one finger applied to the center of the die was the most suitable method to protect the fiber pig tails probably due to flexure of the silicon on the soft polishing pad. The lapping films never produced a mirror quality surface. Figure 19. shows the scratches left after using the hand polishing system.

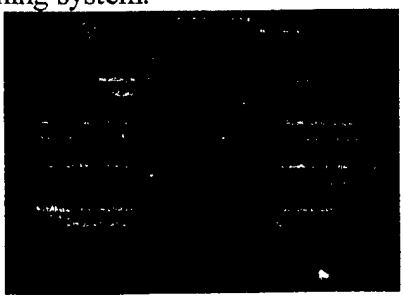

Figure 19. Hand Polished Sample

2.13.2 Ecomet Grinder / Polisher

The Ecomet grinding/polishing system produced better surface quality, but damage to the FAD was difficult to prevent. All attempts to use the Ecomet involved the Automet head to achieve the most repeatable process. The Automet head controlled the pressure of the grinding polishing, and provided a constant rotation of the work. Because the system was developed for preparing potted samples for cross-sectioning, the precision of the pressure setting was in one pound-force (lbf) increments. However, it seems the initial force applied as the chuck is lowered to the wheel is much higher. A noticeable drag in the grind wheel speed is audible before the down-force is stabilized. This was enough to shatter the samples in the first fixture that was developed for grinding the FAD.

As described in Chapter 3, a wafer polishing chuck designed by Michael Palmer was tested for FAD grinding. The FAD was attached to the polishing chuck using Crystalbond™ 509 adhesive on a 125° C hot plate. However, breakage of the silicon die was still observed when the new holder was used. The fit of the holders into the chuck is similar to that of a universal joint and allows the holder to swivel to remain co-planer with the grind wheel. The FAD breakage was occurring when the chuck was lowered as the holder was swiveling into the co-planer position and the down-force was stabilizing. To eliminate this breakage, 0.5 mm stainless steel shims were added to three points on the perimeter of the round holder (Figure 20) to aid in the leveling and to share the down force with the FAD. These greatly slowed the grinding process. This was resolved by cleaving a silicon wafer and using large fragments for the three shims. This fixturing allowed for grinding and polishing of the FAD without destroying the silicon dice.

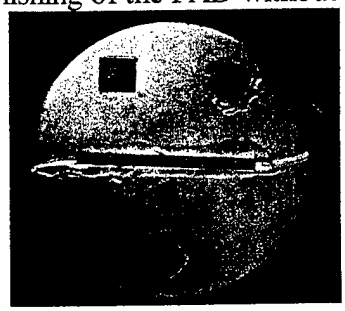

Figure 20. Stainless Steel Shims

Results of polishing with this fixturing were unsuccessful in producing useful dice, however. The optical fiber was consistently becoming detached at the edge of the FAD. Often this was only observable when the FAD was un-mounted from the holder. While glass fiber has a high tensile strength, it has low resistance to shear and bending stresses. Two solutions to this problem were investigated. The first was to machine protective wells into the holder to allow the fiber pig tails to be recessed during the polishing / grinding process. The other was to add extra UV curable epoxy to junction of the fiber pig tails and the edge of the dice.

This resulted in more devices surviving the grinding and polishing process in tact on a macroscopic level. Results from cross-sections discussed in 0 show that the grinding and polishing processes were successful at providing a flat surface for the mounting of the photo detector array and the specified dimensions could be achieved. However microscopic examination of the polished samples revealed additional problems. a shows fractures in a fiber after the grinding and polishing processes. Figure b. shows a section of fiber with missing fragments that were swept away during the grinding and polishing steps. The fracturing was reduced slightly by modifying the grinding process to use Buehler Ultra-prep™ diamond lapping film instead of silicon carbide grinding pads. The diamond particles provide a duller cutting edge than the SiC and are less likely to fracture the glass fiber.

Figure 21a&b Broken Fiber

2.14 Final Testing

Final testing was performed by coupling laser light into each pigtail and checking for throughput and fiber fractures. The Fiber Instrument Sales (FIS) OF-1000S Visible Fault Locator which consists of a battery powered diode laser producing 1 mW of 670 nm light which is made available at a type ST optical fiber connector. The light was transmitted to the pigtail of interest by a connecting a FIS S3-88S-2-FIS single mode patch cord to the fault locator. The patch cord was cut in half and prepared for a splice to the pigtail by stripping and cleaving the cut end of the patch cord. This was accomplished by stripping the tubing and plastic coating 8 mm from the end of the fiber. The stripped portion was placed in a Fitel cleaver which uses a ceramic blade to scribe the fiber about 4 mm from the end. A bending force was applied to cleave the fiber at the scribed location.

The pigtail to be tested was prepared by stripping and cleaving it in the same manner. The pigtail and patch cord were spliced by placing them into a Siecor lab splice. Figure22. shows the fault locator connected to a pigtail through a leaky splice.

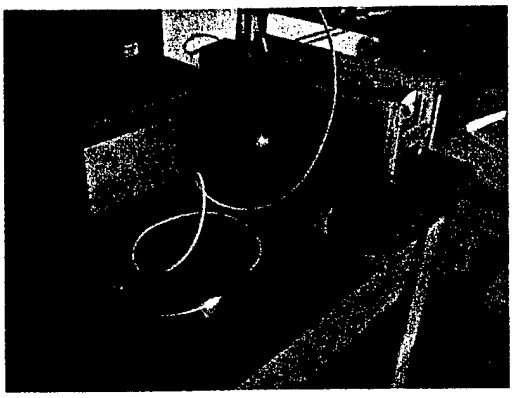

Figure 22. Fault Locator

The testing with the fault locator revealed any fractures in the fiber because light was coupled out at the fractures. There were two main areas that fractures were observed: the transition from the wide to narrow portions of the grooves and at the junction of the pigtail and the wide groove (see figure 23).

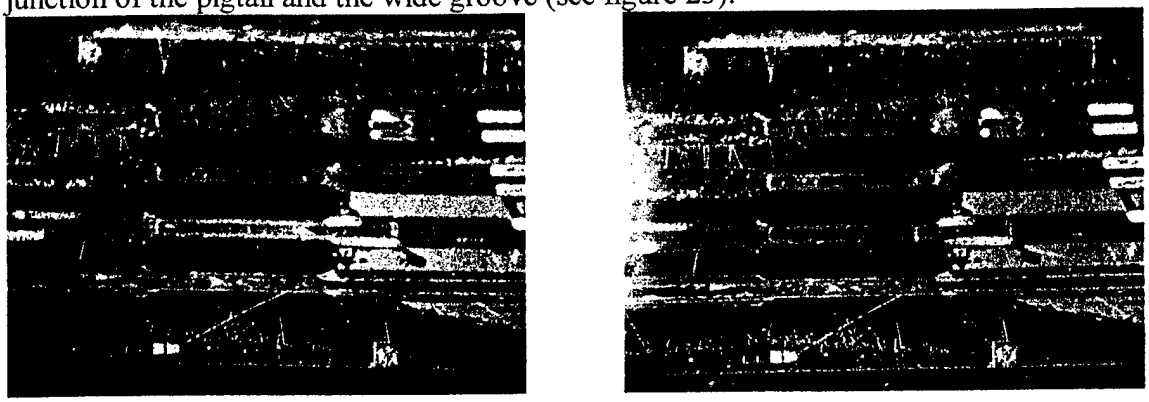

Figure 23a. Fractures at Groove Transition

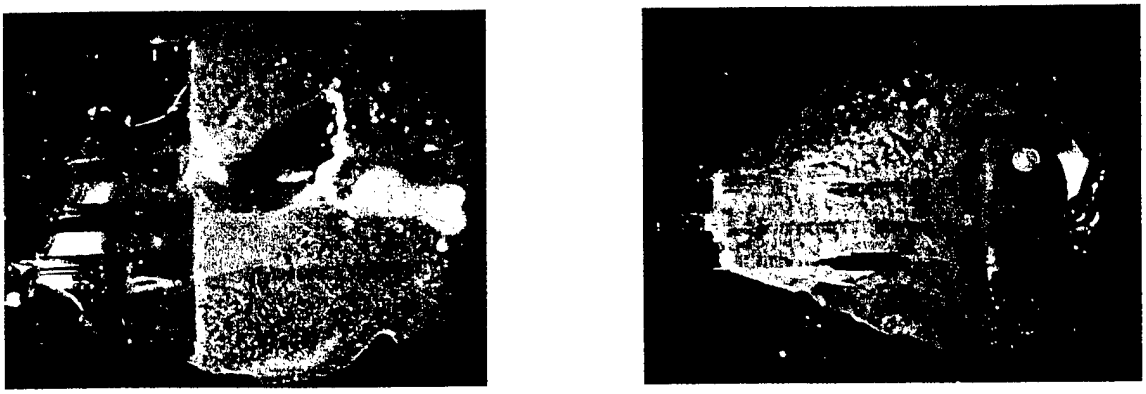

Figure 23b. Fractures at Edge of FAD

The proposed solution for eliminating the fractures at the groove size transition is to eliminate the groove size transition. The use of un-stripped fiber throughout the entire length of the device should be possible with redesigned grooves. The current grinding

process already requires the removal of soft material such as the plastic coating of the fiber along the strain relief portion of the FAD and the UV curable epoxy that is used to secure the fibers.

While most of three wafers were consumed during process development. Five devices were tested and successfully delivered to UAH for Bragg Grating inscription and further testing. The devices were from three wafers. Two etched and diced wafers are available for further process development.

2.15 Conclusions

The fiber attachment device can be produced through the methods described in this work. The FAD parts that were produced should be useful in evaluating subsequent steps in the development of a proof-of-concept model for the Simultaneous Optical Multiprocessor Exchange Bus.

While several parts were produced that meet the dimensional specifications for the SOME Bus project, yield was low. Six tested parts were delivered out of five wafers processed.

2.15.1 Suggestions for Future Work

In order to improve quality of future devices, a new mask set should be designed. The first mask should provide a method of aligning subsequent masks to the crystal orientation of the wafer. This method is described in previous chapters and involves opening circular windows in the Silicon Nitride hard mask and performing a short KOH etch to make the edges of the {111} planes visible.

It is also suggested that the V-groove etch window mask be redesigned to eliminate the narrow portion of the grooves. This would eliminate the need to strip the plastic coating from any portion of the fiber and eliminate the fiber breakage that occurs at the transition from wide to narrow grooves.

Options for obtaining a more uniform silicon nitride mask layer should be explored. This would improve the surface quality of the FAD.

To improve yield, more control must be obtained in the grinding and polishing process. In particular, the pressure applied by the chuck as it moves into position must be better controlled. Since discussions with Buehler revealed that they believe the machine is operating properly, the Ecomet machine may not be appropriate for this type of work. An additional suggestion for grinding and polishing is to replace the shims on the work holder with a round silicon wafer with a slot removed to receive the FAD.

REFERENCES

[1] J. Kulick, "The simultaneous optical multiprocessor exchange bus," in *Proc. IEEE Conf. on Massively Parallel Processor Optical Interconnects,* 1995, pp 336-344.

Fabrication of Slanted Fiber Bragg-gratings

A. Sharma
Department of Physics, Alabama A&M University, Normal, AL-35762

Final Report for SUB2000-366

A Subcontract from University of Alabama, Huntsville

Abstract

The Subcontract SUB2000-366 from University of Alabama, Huntsville, involved development of techniques to fabricate slanted Bragg-gratings in single-mode optical fibers. An expertise for fabricating such gratings for any required slant angle was developed. This report describes the technique and the results. Fiber-optic Bragg grating filters are fabricated with a range of Bragg wavelength between 1296 and 1336 nm, using a single phase mask. 30-50 mW of continuous-wave light at 244 nm is used from a frequency-doubled argon-ion laser having an intracavity etalon. For small slant angles up to 15°, gratings are fabricated by rotating the photosensitive fiber about a vertical axis with respect to the phase mask. For higher tilt angles all the way up to 45°, the fiber is rotated about a horizontal axis along the laser beam direction. The variation of Bragg wavelength with the fiber-tilt is explained with a simple formula. High spatial coherence of 244 nm light makes it possible to displace the fiber as much as 6 mm in front of the phase mask and tilt the fiber by as much as 15 degrees.

Introduction

Since their discovery[1] in 1978, fiber-optic Bragg gratings have been used for numerous applications in the area of sensing[2-4] and light-based communication[5-7]. Several techniques are available[8-12] to fabricate these gratings with a range of properties. Out of all of these techniques, the one involving use of a phase-mask[9] is the simplest since the constraints of mechanical stability of fabrication set up and coherence of light are much reduced. The disadvantage of this technique is that, unlike other interferometric techniques, phase masks can be used to fabricate normal gratings of only single Bragg wavelengths, with grating planes perpendicular to the fiber-axis. It was shown recently that by varying the angle between the fiber and the phase-mask[10], one could fabricate tilted gratings, which have all the properties of a normal grating, for use in applications ranging from sensing to optical communication. The maximum tilt angle in the above-referenced paper was about 3°, resulting in Bragg wavelength that could be varied within a range of 2 nm around a wavelength of 1.56 μm. As described later, greater spatial coherence of light source used in this work enables us to tilt the fiber by as much as 15° along a horizontal plane, resulting in a corresponding variation of Bragg wavelength in a 40 nm range around 1.32 μm. Thus, a single phase mask has been used by us to fabricate several gratings with wavelengths between 1296 and 1336 nm, reflectivity varying between 10-100% and filter bandwidth around 0.4 nm. Due to small tilt angles for fiber rotated in the horizontal plane, the Bragg reflected light is essentially recoupled into the fiber core, resulting in gratings that effectively function as normal gratings. To couple light out of the fiber, a much greater tilt angle is required. This is possible by rotating the fiber in a vertical plane. Several such slanted gratings were fabricated such that light is coupled out at angles around 90° to the fiber-axis.

Experimental Technique

Figure 1 shows a schematic of the experimental set up used in this work. Figure 1a shows the set up for small tilt angles and 1b for large tilt angles up to 45°.

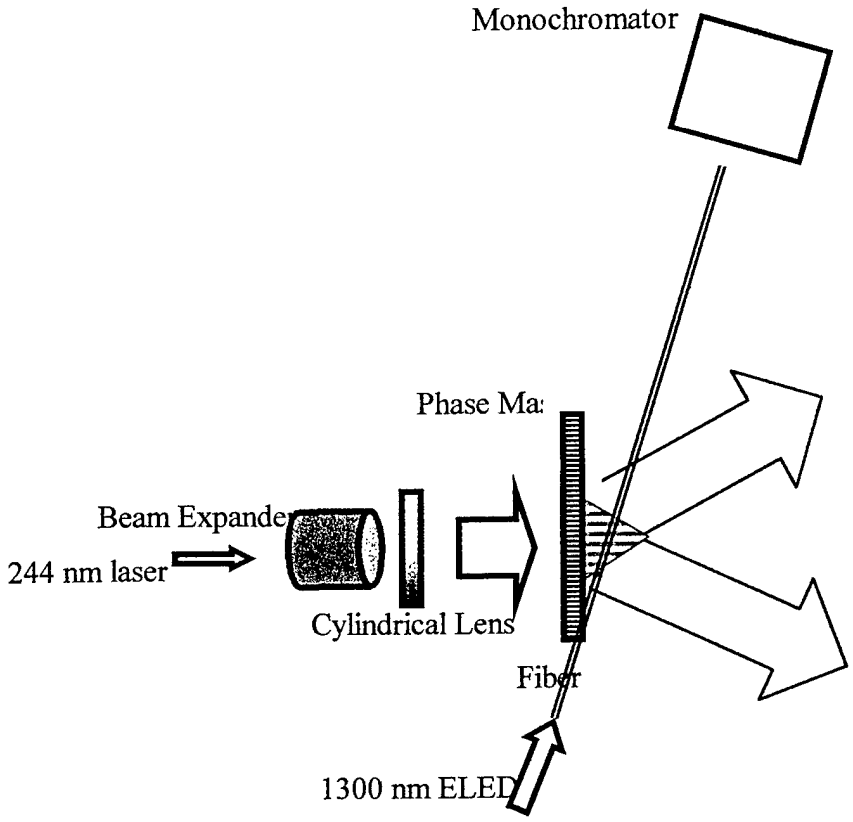

Figure 1a: Schematic of the experimental set up to fabricate tilted Bragg gratings up to a tilt angle of 15°. A frequency-doubled argon-ion laser at 244 nm is used. Angle of tilt, θ between the phase mask and the fiber can be varied between 0-15 degrees. The transmission spectrum of the gratings is obtained in real time using a broadband 1300 nm ELED as a light source.

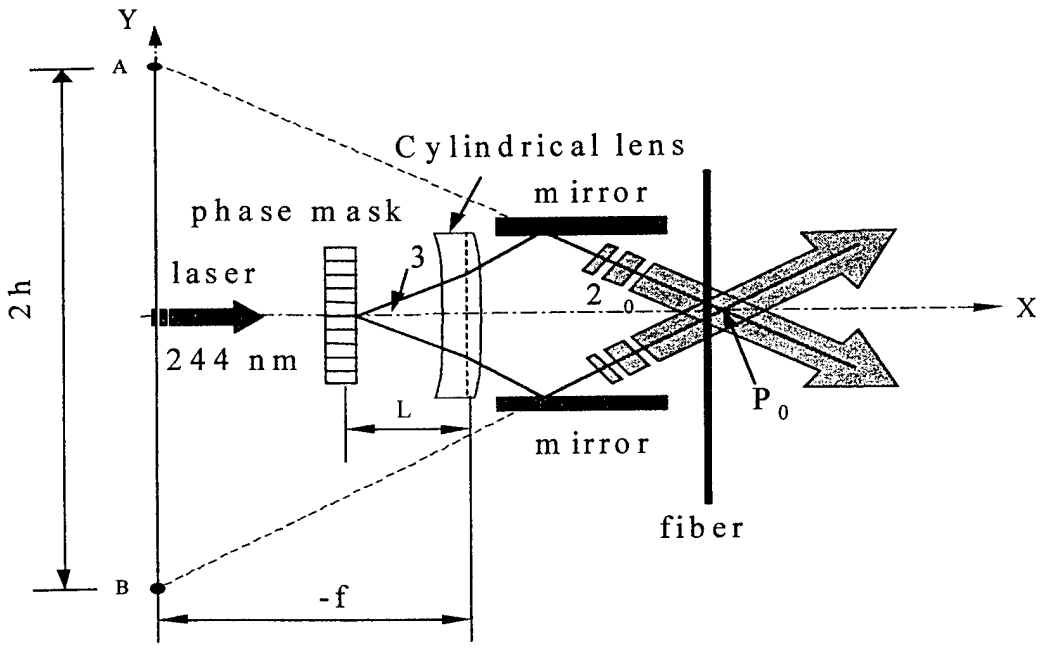

Figure 1b. Talbot interferometric set up that was used to fabricate slanted Bragg gratings for large tilt angles up to 45°. 244 nm UV light source was used to write gratings. A and B are virtual light sources. Bragg wavelength can be changed by a simple translation of fiber and/or tilting the two mirrors. The fiber can be rotated by any angle in a vertical plane, about the X-axis (laser beam-axis)

The source of light used for fabricating slanted Bragg gratings is a continuous wave, frequency-doubled argon-ion laser of 244 nm wavelength and power of 30 mW. An intracavity etalon results in a narrow laser linewidth of less than 10 MHz. Photosensitive optical fibers with a high concentration of germania as well as ordinary communication-grade fiber are used in this work. The former have a core diameter of 2.3 μm and a cutoff wavelength of 0.83 μm, while the latter have a core diameter of around 8 μm. Additionally, for large slant angles around 45°, D-fibers were used. Prior to writing gratings, the fibers are hydrogen loaded in 1000 psi pressure for about a week. The 1 mm diameter ultraviolet (UV) light can be expanded with a 10X beam expander and focused on the fiber with a cylindrical lens perpendicular to the plane of figure. The fiber is placed in front of the phase-mask as shown. The phase mask used in this work has a period of 890 nm (QPS) and physical dimensions of 10 mm x 3 mm. The light in the 0^{th} grating order is only about 2% and about 36% in each of the first orders, which are diffracted at angles of about 16 degrees with respect to the incident UV light direction. By rotating the fiber in a horizontal plane, the tilt angle between the phase-mask and the

fiber, θ can be varied between 0 and 15 degrees. In this case, the center of the fiber where the Bragg grating is fabricated is always maintained at a distance of 6mm in front of the phase mask even as the fiber is tilted. Such geometry ensures that the length of Bragg grating does not change much as the tilt angle is varied. This can be compared to a maximum displacement of only about 500 μm in an earlier experiment[10] using KrF excimer laser, even with an intracavity etalon to improve its spatial coherence. Superior spatial coherence of the single-mode argon-ion laser makes it possible to displace the fiber by 6 mm in front of the phase mask and tilt the fiber by as much as 15 degrees as compared to just 3 degrees in the earlier work. Several Bragg gratings are fabricated in this work with tilt angle of the fiber increased in increments of 2-3 degrees. The Bragg wavelength of the fiber-grating is related to the fiber tilt and can be varied over a range of 40 nm as compared to just 2 nm in earlier work. Typical time for fabricating the Bragg gratings is about 2-10 minutes.

For small tilt angles, the reflectivity of the Bragg gratings is measured in real time with a 0.85 m double monochromator (SPEX 1404) in conjunction with an InGaAs detector and a lock-in amplifier. A broadband edge light emitting diode (ELED) with a bandwidth of 50 nm and central wavelength of around 1300 nm is used for this purpose. For large tilt angles around 45°, the slanted grating is fabricated for He-Ne laser wavelength of 633 nm. Visible light makes it easier to study the characteristics of the light coupled out of the fiber.

Measurement and Analysis:

Figure 2 shows transmission curves for several Bragg gratings fabricated by tilting the fiber at different small angles.

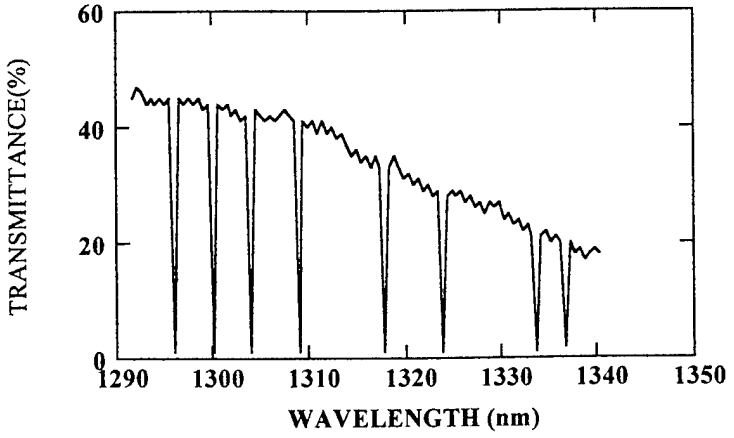

Figure 2
Transmission spectrum of eight different tilted Bragg gratings made with same phase mask. As the tilt angle is changed from 0 to 15 degrees, the Bragg wavelength varies between 1296.1 and 1336.7 nm. The bandwidth of each of these grating filters is around 0.4 nm (FWHM) while the maximum reflectivity is around 100%.

Due to small tilt angles, the Bragg reflected light is recoupled into the core and the grating behaves like a normal grating. In each of the cases the reflectivity of Bragg grating is about 95-100%. The time to fabricate these gratings varies from about 2 minutes at 0 degree tilt to 10 minutes at 15 degree tilt. The reflectivity of gratings as they are fabricated is shown in figure 3.

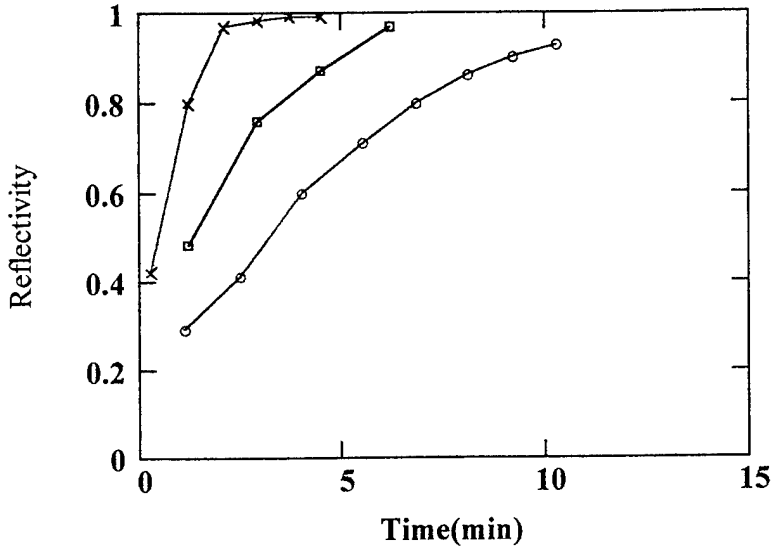

Figure 3. Variation of grating reflectivity in real time as it is being fabricated. For three tilt angles of 0, 6 and 14 degree, the experimental points are represented by (x), (□) and (o) respectively.

As seen in figure 2, the Bragg grating reflection filter bandwidth is about 0.4 nm (FWHM) for all tilt angles between 0 and 15 degrees. The numbers for reflectivity can be compared to earlier work[10] in which the reflectivity gradually decreases from 80% to 0% as the tilt angle is increased from 0 degree to 3 degree. Near 100% reflectivity of gratings in our work is due to the greater spatial coherence of argon-ion laser light, which permits fiber displacement of 6 mm from the phase mask. The constant displacement of fiber of 6 mm from the phase mask ensures a Bragg grating of almost constant length. These Bragg gratings are formed in the shaded region of figure 1, where the two first-order-diffracted beams from phase mask overlap. Calculated length of grating for different tilt angles and consequently, its bandwidth essentially remains constant as the tilt angle is changed from 0 degree to 15 degree.

Measured value of Bragg wavelength for different angles of fiber tilt is shown in figure 4. Bragg wavelength varies from 1296.1 nm when fiber is parallel to phase mask (tilt angle of 0 degree) to 1336.7 nm when fiber is tilted at an angle of 15 degrees with respect to the phase mask. The four gratings with Bragg wavelengths between 1296 and 1310 nm are all fabricated in the same fiber while others are in different fiber segments.

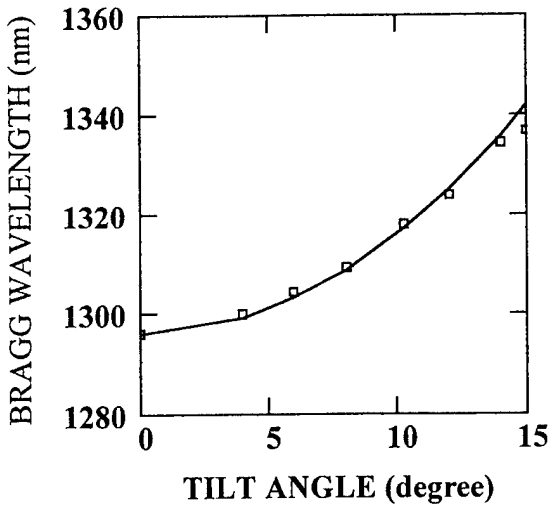

Figure 5. Variation of measured Bragg wavelengths with the fiber-tilt. The solid line is given by the theoretical expression in equation (1)

Relation between the Bragg wavelength (λ) and the fiber-tilt angle (θ) is given by a simple equation[10],

$$\lambda(\theta) = \lambda(0)/\cos(\theta) \quad \ldots\ldots\ldots\ldots\ldots\ldots\ldots\ldots (1)$$

where, $\lambda(0) = 1296.1$ is the Bragg wavelength when fiber is parallel to phase mask. Equation (1) is also plotted in figure 4. As can be seen here the agreement between measured values of Bragg wavelengths and equation (1) is good.

For slanted Bragg gratings at tilt angles of around 45°, the Talbot interferometer shown in figure 1b is used for fabrication. These gratings are fabricated for 633 nm wavelength of a He-Ne laser. Photographs showing light coupling out of the side of the fiber for 45° tilted grating are shown in figures 5 and 6. Maximum out-coupling efficiency of around 1% has been achieved. Such gratings have been made in a variety of fibers: photosensitive and communications grade single-mode fibers, D-fibers and also few-mode fibers.

Conclusion

We have developed techniques for fabricating slanted fiber-optic gratings at any wavelength and tilt-angle, using a single phase-mask. The technique is demonstrated by fabricating several slanted gratings around 1300 and 633 nm regions in several different types of fibers and with different slant-angles. The Talbot interferometer used in this work is convenient to fabricate gratings with desired parameters.

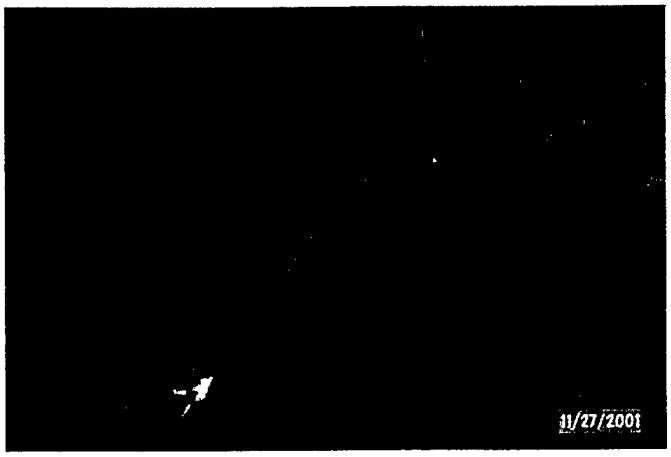

Figure 5. Photograph to show outcoupling of He-Ne laser light by a 45° slanted grating in a D-fiber. The He-Ne light source is to the right of photograph. The white spot in the middle of fiber is due to a very directional light beam towards the camera and is the location of slanted Bragg grating. Some of the out-coupled light is reflected back on the screen and appears as a streak with an angular spread of less than 1° along the fiber axis.

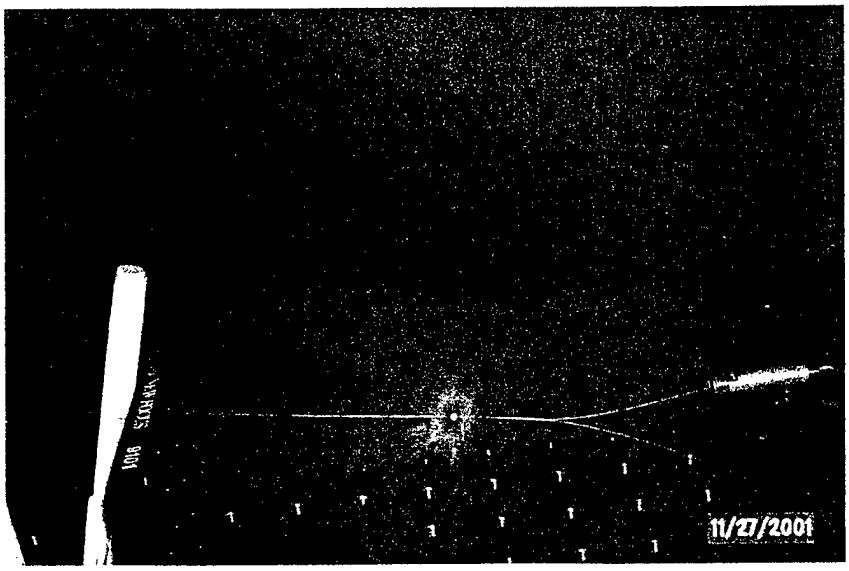

Figure 6. Photograph to show outcoupling of He-Ne laser light by a 45° slanted grating in a D-fiber. The He-Ne light source is to the right of photograph. The white spot in the middle of fiber is due to a very directional light beam towards the camera and is the location of slanted Bragg grating.

List of refereed articles and conference proceedings supported by this grant:

1. A technique for fabrication of fiber-optic grating filter over a wide range of Bragg wavelength and bandwidth using a single phase mask
   Y. Wang, J. Grant and A. Sharma, Journal of Lightwave Technol. **19**, 1569 (2001)

2. Enhanced growth rate for Bragg grating fabrication in optical fibers with titania-doped outer cladding.
   Y. Wang, L. Phillips, C. Yelleswarapu, T. George, A. Sharma, S. Burgett, and P. Ruffin, Optics Communications **163**, 185 (1999)

3. Fabrication of fiber-optic Bragg gratings: effect of ultraviolet light absorption by the fiber buffer.
   Y. Wang, J. Grant and A. Sharma, Applications of Photonics Technology 4, Proceedings of SPIE Vol. 4087 (2000), 150

4. Fabrication of a fiber-optic tilted Bragg grating in 40 nm range with a single phase-mask.
   J. Grant, Y. Wang, and A. Sharma, PhotonicsNorth, June 3-6, 2002 (Quebec City, Canada)

List of students graduated with partial support from this grant:

1. Fabrication of Bragg gratings in optical fibers and their application as strain sensors in fiber-optic coils.
   Leon A. Phillips III, Ph.D., July 2000

2. Fiber Bragg gratings: Characterization of some novel fabrication techniques.
   Ying Wang, Ph.D., April 2001

References

[1] B. S. Kawasaki, K. O. Hill, D. C. Johnson, and Y. Fujii, Opt. Lett. 3 (1978) 66

[2] I. Bennion, J. A. R. Williams, L. Zhang, K. Sugden, and N. J. Doran, Opt. Quant. Electron. 28 (1996) 93

[3] Y. J. Rao, D. A. Jackson, L. Zhang, and I. Bennion, Opt. Lett. 21 (1996) 683

[4] M. LeBlanc, S. Y. Huang, M. Ohn, R. M. Measures, A. Guemes, and A. Othonos, Opt. Lett. 21 (1996) 1405

[5] X. J. Gu, Opt. Lett. 23 (1998) 509

[6] A. Galvanauskas, D. Harter, M. A. Arbore, M. H. Chou, and M. M. Fejer, Opt. Lett. 23 (1998) 1695

[7] B. J. Eggleton, T. Stephens, P. A. Krug, G. Doshi, Z. Brodzeli, and F. Ouellette, Electron. Lett. 32 (1996) 1610

[8] G. Meltz, W. W. Morey, and W. H. Glenn, Opt. Lett. 14 (1989) 829

[9] K. O. Hill, B. Malo, F. Bilodeau, D. C. Johnson, and J. Albert, Appl. Phys. Lett. **62** (1993) 1035

[10] A. Othonos, and X. Lee, IEEE Photonics Tech. Lett. **7** (1995) 1183

[11] H. Patrick, and S. L. Gilbert, Opt. Lett. 18 (1993) 1484

[12] Y. Wang, L. Phillips, C. Yelleswarapu, T. George, A. Sharma, S. Burgett, and P. Ruffin, Opt. Comm. **163** (1999) 185